Global Screening of Base Excision Repair in Nucleosome Core Particles

Treshaun B. Sutton[1], Danielle L. Sawyer[2], Tasmin Naila[3], Joann B. Sweasy[4], Alan E. Tomkinson[3], and Sarah Delaney[1,*]

[1]Department of Chemistry, Brown University, Providence, Rhode Island 02912, United States

[2]Department of Cellular and Molecular Medicine, University of Arizona, Tucson, Arizona 85724, United States

[3] Departments of Internal Medicine, Molecular Genetics & Microbiology, and the University of New Mexico Comprehensive Cancer Center, University of New Mexico Health Sciences Center, Albuquerque, New Mexico 87131, United States

[4]Eppley Institute for Research in Cancer and Allied Diseases, Fred & Pamela Buffett Cancer Center, University of Nebraska Medical Center, Omaha, Nebraska 68198, United States

Keywords: Nucleosome core particle; Base excision repair; DNA glycosylase; AP Endonuclease 1; Polymerase β; LigIIIα/XRCC1

ABSTRACT

DNA damage is a fundamental molecular cause of genomic instability. Base excision repair (BER) is one line of defense to minimize the potential mutagenicity and/or toxicity derived from damaged nucleobase lesions. However, BER in the context of chromatin, in which eukaryotic genomic DNA is compacted through a hierarchy of DNA-histone protein interactions, is not fully understood. Here, we investigate the activity of BER enzymes at 27 unique geometric locations in a nucleosome core particle (NCP), which is the minimal unit of packaging in chromatin. The BER enzymes include uracil DNA glycosylase (UDG), AP endonuclease 1 (APE1), DNA polymerase β (Pol β), and DNA ligase IIIα complexed with X-ray repair cross complementing group 1 (LigIIIα/XRCC1). This global analysis of BER reveals that initiation of the repair event by UDG is dictated by the rotational position of the lesion. APE1 has robust activity at locations where repair is initiated whereas the repair event stalls at the Pol β nucleotide incorporation step within the central ~45 bp of nucleosomal DNA. The final step of the repair, catalyzed by LigIIIα/XRCC1, is achieved only in the entry/exit regions of the NCP when nick sites are transiently exposed by unwrapping from the histones. Kinetic assays further elucidate that the location of the damaged lesion modulates enzymatic activity. Notably, these data indicate that some of the BER enzymes can act at a significant number of locations even in the absence of chromatin remodelers or other cellular factors. These results inform genome wide maps of DNA damage and mutations and contribute to our understanding of mutational hotspots and signatures.

Abbreviations

APE1, AP endonuclease 1; BER, base excision repair; 5'-dRP, 5'-dRP; LigIIIα, DNA ligase IIIα; FD, free duplex DNA; FEN1, flap endonuclease 1; FPLC, fast protein liquid chromatography; HRF, hydroxyl radical footprinting; IPTG, isopropyl β-D-1-thiogalactopyranoside; LB, Luria broth; NCP, nucleosome core particle; PARP, poly(ADP-ribose) polymerase; PCI, phenol/chloroform/isoamyl alcohol; Pol β, DNA polymerase β; PMSF, phenylmethylsulphonyl fluoride; SE, standard error; SAFA, semi-automated footprinting analysis; STO, single turnover; U, uracil; UDG, uracil DNA glycosylase; WT, wild type; XRCC1, X-ray repair cross complementing group 1

1. Introduction

Genomic DNA is constantly exposed to a variety of endogenous and exogenous damaging agents. To maintain genetic integrity, cells have several pathways for recognition and removal of DNA damage. One of these pathways, base excision repair (BER), is responsible for repairing damaged nucleobase lesions [1-3]. To initiate BER, a DNA glycosylase excises the lesion by cleaving the N-C1' glycosidic bond between the deoxyribose sugar and the lesion, generating an abasic site (Figure 1A). There are both monofunctional and bifunctional DNA glycosylases. A monofunctional glycosylase generates an abasic site, while a bifunctional glycosylase additionally incises the sugar-phosphate backbone producing either a phosphate or polyunsaturated aldehyde at the 3'-end of the gap, and a 5'-phosphate.

Following a monofunctional glycosylase, AP endonuclease 1 (APE1) incises the sugar-phosphate backbone 5' to the abasic site. In short-patch BER, DNA polymerase beta (Pol β) acts next and has two functions: removing a 5'-deoxyribose phosphate (5'-dRP) and incorporating an undamaged deoxynucleotide. Lastly, DNA ligase IIIα (LigIIIα), in complex with X-ray repair cross complementing group 1 (XRCC1), completes the repair by sealing the nick in the backbone. In cases where the 5'-dRP is chemically modified, it may be refractory to the 5'-dRP lyase activity of Pol β [4]. In these instances, long-patch BER is used. Pol β or another DNA polymerase performs strand displacement synthesis where 2-13 nucleotides are filled into the gap, the displaced flap of DNA is removed by flap endonuclease 1 (FEN1), and DNA ligase I seals the nick to complete the repair. In the case of a gap produced by a bifunctional DNA glycosylase, APE1 or polynucleotide kinase convert the ends to enable Pol β to incorporate a deoxynucleotide and LigIIIα/XRCC1 completes the repair event.

There is evidence that the activity of BER enzymes is coordinated in a way that has been likened to the passing of a baton in a relay race [5]. This coordination, or substrate-product channeling between the BER enzymes, can prevent exposure of toxic and mutagenic repair intermediates [6], [7]. Scaffolding proteins have also been shown to assist this coordination by providing a platform for BER enzymes to assemble and localize to their respective substrates [8-11].

The molecular mechanism for each of the BER enzymes and how they accomplish repair on duplex DNA is well established. However, eukaryotic DNA is packaged in chromatin and how BER is accomplished on packaged DNA is less well defined. The most basic unit of packaging is the nucleosome core particle (NCP). The NCP is comprised of 145-147 base pairs (bp) of DNA wrapped around an octameric protein core containing two copies each of histone proteins H2A, H2B, H3, and H4 (Figure 1B) [12]. There is also a two-fold axis of pseudo-symmetry in an NCP called the dyad axis. Much of the biochemical research on NCPs has used positioning DNA sequences, in which the DNA binds to the histone proteins in a reproducible orientation. These positioned NCPs provide chemically and structurally well-defined substrates for biochemical assays of BER. Notably, positioned NCPs are well documented *in vivo* [13-15].

Previous studies have explored the activity of BER enzymes on NCPs. These studies revealed that the geometric position of the lesion can impact its ability to be recognized by DNA glycosylases and the downstream BER enzymes (please see recent reviews [16-18]). For example, lesions with a rotational position facing out towards solution (Figure 1B), as opposed to facing in towards the histone core, are more readily excised by DNA glycosylases. The translational position of a lesion can also influence BER with DNA in the entry/exit region being prone to transient and spontaneous unwrapping from the histones. This increased dynamics has been shown to facilitate

access to sterically-occluded lesions [19-21]. Parameters such as the proximity of a lesion to the unstructured N-terminal histone tails or an adjacent DNA superhelix can also modulate the activity of BER enzymes on the NCP.

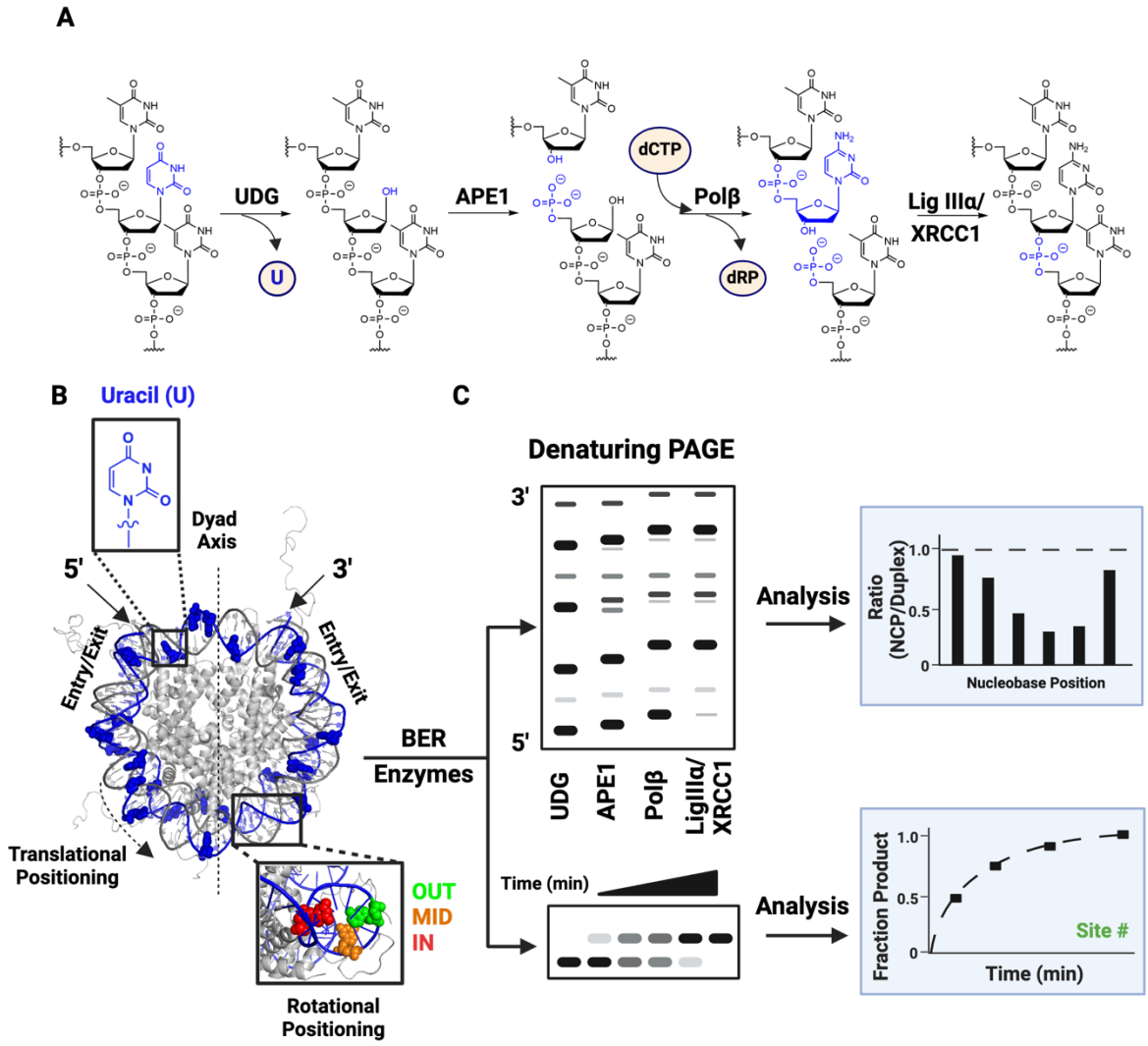

Figure 1. Overview of BER pathway and workflow of repair activity assessment on NCPs. (A) Overview of the BER pathway initiated by a monofunctional DNA glycosylase. Regions highlighted in blue reflect changes occurring throughout the repair process. (B) Representation of an NCP created by merging PDB: 3lz0 (an NCP containing Widom 601 DNA) and PDB: 1kx5 (an NCP including histones with N-terminal tails). Blue space-filling representation indicates the global substitution of cytosine to uracil on the "J strand" of 601 DNA. Entry/exit region and dyad axis are indicated. Inset (top) is the chemical structure of uracil. Inset (bottom) highlights the rotational positions: OUT (green), MID (orange), and IN (red). (C) Schematic representation of denaturing PAGE analysis of the BER pathway on NCPs (top) and a schematic representation of a time course experiment analyzing kinetic activity of a single BER enzyme (bottom).

While this prior work provided significant insights into the ability of BER to be accomplished in chromatin, many of the studies were limited to probing repair at only a few lesion sites. Indeed, previous research has shown that repair is quite sensitive to the local environment of a lesion and, thus, a more comprehensive characterization of repair in NCPs is needed. Here we used the repair fingerprinting technique developed previously in our laboratory [22] to investigate short-patch BER at 27 unique rotational and translational locations in a positioned NCP (Figure 1C). Uracil (U) was used as a well-known and prototypic substrate lesion for BER. The repair event was initiated by excision of U by uracil DNA glycosylase (UDG) which is a monofunctional glycosylase known to remove U paired with A or G [23]. The activity of UDG, APE1, Pol β, and a LigIIIα/XRCC1 complex was determined at each U lesion. Kinetic assays provide a quantitative description of enzymatic activity. Taken together, the results describe the ability of BER to be accomplished in a positioned NCP and define geometric locations where BER can be initiated, locations where BER stalls at one of the intermediate steps in the pathway, and locations where repair can be successfully completed. The results can inform observations of genomic DNA damage profiles and contribute to our understanding of mutational hotspots and signatures.

2. Materials and Methods

2.1 Oligonucleotide synthesis and purification

All DNA was synthesized using phosphoramidite chemistry on a MerMade 4 DNA synthesizer (BioAutomation). Phosphoramidites and DNA synthesis reagents were purchased from Glen Research. The 145mer oligonucleotide containing global C to U substitution (Scheme S1) was prepared using methods reported previously [24]. A Poisson distribution ($\lambda = 0.355$) was used to determine the molar ratio of C to U such that 95% of the oligonucleotides contain at most one U per strand. Both the 145mer oligonucleotide containing the C to U substitution (J strand) and

the complementary 145mer (I strand) were purified by 8% denaturing polyacrylamide gel electrophoresis (PAGE). To confirm the global substitution of C to U, single-stranded 145mer J strand was 5'-^{32}P-end radiolabeled using T4 PNK kinase (New England Biolabs) and incubated with UDG (New England Biolabs) for 30 min at 37 °C. Resulting abasic sites were converted to strand breaks by incubation with NaOH for 2 min at 90 °C, dried *in vacuo*, analyzed by both 8 and 10% denaturing PAGE, and imaged by phosphorimagery.

Two internal standards (27mer and 118mer; Scheme S1) were designed to not co-migrate with any of the expected BER products when analyzed by denaturing PAGE. The 27mer and 118mer were purified by 8 and 12% denaturing PAGE, respectively.

2.2 Histone preparation and NCP reconstitution

Xenopus laevis histone octamer was purchased from the Histone Source. NCPs were reconstituted via salt-gradient dialysis as previously described [25]. Briefly, 145mer J strand was 5′-^{32}P-end radiolabeled and annealed to its complement (145mer I strand) in annealing buffer (10 mM Tris [pH 8], 50 mM NaCl). 1 μM radiolabeled duplex DNA was combined with 2 μM histone octamer in a Slide-a-Lyzer dialysis device (0.1 mL capacity, 3.5 kDa, Thermo Fischer Scientific) in 200 mL (2 M NaCl, 10 mM Tris [pH 8], 1 mM EDTA, 1 mM DTT and 0.5 mg/mL BSA). Samples were incubated at 4 °C and the NaCl concentration was reduced stepwise at ~1 h intervals (1.2 M, 1.0 M, 0.6 M) via dialysis. The final dialysis to 0 M NaCl was for 3 h. Samples were filtered by centrifugation using a Spin-X Centrifuge Tube filter (0.22 μM, Corning Incorporated) to remove precipitates. To determine purity, samples were analyzed by 7% native PAGE (19:1 acrylamide:bisacrylamide, 0.25X TBE) at 4 °C for 3 h at 160 V. Only NCPs containing ≤ 5% duplex DNA were used in subsequent experiments.

2.3 Hydroxyl radical footprinting (HRF)

HRF reactions were performed on NCP samples based on previously published methods [26]. In short, 7.5 µL each of 10 mM Fe(II)EDTA, 10 mM sodium ascorbate, and 0.12% v/v aqueous hydrogen peroxide were combined and immediately added to 5 pmol of NCP in 52.5 µL reaction buffer (10 mM Tris [pH 8], 1 mM EDTA). The sample was incubated at 37 °C for 5 min and the reaction was quenched with 16 µL 50 mM EDTA in 25% v/v glycerol. NCPs were immediately loaded onto a 7% native PAGE (19:1 acrylamide:bisacrylamide, 0.25X TBE) to separate NCPs from duplex DNA that dissociated during the HRF reaction, and electrophoresed at 4 °C for 3 h at 160 V. The NCP band was then excised from the gel and eluted in gel elution buffer (0.3 M NaOAc, 1 mM Tris [pH 8], 1 mM EDTA) for 22 h at 37 °C and gentle shaking (60-70 rpm). Samples were concentrated using a 30 kDa MWCO concentrator filter (Millipore) for 15 min at 4,000 rpm. The concentrated samples were extracted twice with 400 µL phenol:chloroform:isoamyl alcohol (PCI; 25:24:1) to remove proteins and the DNA was ethanol precipitated using 50 µL precipitate solution (0.3M NaOAc, 0.5 mg/mL tRNA, 1 mM EDTA) and cold 200 proof ethanol. DNA fragments were resuspended in 1:1 formamide:deionized water, split in half, and half loaded onto a 10% denaturing PAGE gel to resolve nucleobases -129 to -76 while the other half was loaded onto an 8% denaturing PAGE gel to resolve nucleobases -76 to -8. A/G Maxam-Gilbert sequencing ladders were run alongside the HRF samples. Gels were imaged by phosphorimagery and bands were quantified using semi-automated footprinting analysis (SAFA) software [27]. The rotational position of each nucleobase was established by first identifying the highest HRF reactivity within each helical turn of the nucleosomal DNA. The ratio of band cleavage intensity at each nucleobase within the helical turn was determined by dividing the HRF value at a particular nucleobase by the highest HRF reactivity within the helical turn. Nucleobases

with a ratio greater than 0.8, $0.8 \leq x \leq 0.2$, and less than 0.2 were categorized as OUT, MID, and IN rotational positioning, respectively.

2.4. DNase footprinting

2.5 pmol of duplex or NCPs were treated with 0.02 or 0.002 units of DNase I (New England Biolabs) in reaction buffer (10 mM Tris-HCl (pH 7.6), 2.5 mM $MgCl_2$, and 0.5 mM $CaCl_2$) in a final volume of 25 µL. Samples were incubated for 5 min at 37 °C. Reactions with duplex DNA were quenched by the addition of 12.5 µL 100 mM EDTA and 1 mg/mL calf-thymus DNA. Reactions with NCP samples were quenched by the addition of 8.3 µL 50 mM EDTA, 0.5% SDS, 0.2 mg/mL Proteinase K (ThermoFisher Scientific) and incubation at 55 °C for 2 h. NCP samples were extracted with PCI as described above. All samples were subjected to ethanol precipitation by addition of 50 µL precipitate solution (0.3M NaOAc, 0.5 mg/mL tRNA, 1 mM EDTA) and cold 200 proof ethanol. DNA fragments were resuspended in 1:1 formamide:deionized water, split in half, and half loaded onto a 10% denaturing PAGE gel to resolve nucleobases -129 to -74 while the other half was loaded onto an 8% denaturing PAGE gel to resolve nucleobases -74 to -9. Gels were imaged by phosphorimagery.

2.5 BER proteins

UDG and human APE1 were from New England Biolabs. The total protein concentrations were determined using the Bradford assay with a γ-globulin standard (Bio-Rad Laboratories).

Pol β expression and purification. A pET28a-human wild-type (WT) Pol β-tagless expression vector with kanamycin resistance was used for protein expression, as previously described [28]. Plasmids expressing WT Pol β were transformed into *Escherichia coli* Rosetta DE3 cells for recombinant protein expression and selected with kanamycin (50 µg/mL) and

chloramphenicol (20 μg/mL). Pools of cells were grown in Luria broth (LB) with kanamycin (50 μg/mL) and chloramphenicol (20 μg/mL) at 37 °C to an OD600 of 0.6-0.8 before induction with 1 mM isopropyl β-D-1-thiogalactopyranoside (IPTG) as described. Induced cultures were incubated at 200 rpm for 18 h at 18 °C and pelleted. Pelleted cells were resuspended in 10 mL of Buffer A (50 mM HEPES, 100 mM NaCl, 1 mM EDTA, 2 mM fresh DTT, pH 7.4 and 0.45 μm filter sterilized) with EDTA-free protease inhibitor cocktail (Roche) and 1 mM phenylmethylsulphonyl fluoride (PMSF). After resuspension, bacterial lysis was performed by five rounds of sonication for 30 sec. The soluble fraction was separated by centrifugation at 12,200 g for 30 min at 4 °C. The sample was filtered using a 0.45 μm filter and was loaded onto a BioRad Fast Protein Liquid Chromatography (FPLC) instrument. Buffer A and Buffer B (50 mM HEPES, 2 M NaCl, 1 mM EDTA, 2 mM fresh DTT, pH 7.4 and 0.45 μm filter sterilized) were used for the FPLC fractionation. The sample was loaded onto a 5 mL HiTrap heparin HP column (Cytiva) and fractionated using a low to high salt gradient (Buffer A / Buffer B). Fractions containing Pol β were then concentrated to 1 mL volume using a centrifugal concentrator (Amicon Ultra Centrifugal Filter, 10 kDa MWCO) and diluted with 9 mL of Buffer A prior to being reloaded on the FPLC instrument and applied to a HiTrap SP HP column (Cytiva) for further fractionation. Fractions containing Pol β were concentrated as described above and resolved on a 12% SDS-PAGE gel. The gel was stained with Coomassie blue to assess for protein purity greater than 95%. Protein concentration was measured using a nanodrop (Thermo Fisher) to measure the A280, and the extinction coefficient of Pol β (ε = 21,200 M^{-1} cm^{-1}) was used to calculate the final concentration. Purified Pol β protein was flash frozen in liquid nitrogen and stored in 15% glycerol at -80 °C.

The LigIIIα/XRCC1 complex was expressed and purified as described [29] except that the double-stranded DNA cellulose step was omitted. The total protein concentration was determined

using the Bradford assay with a γ-globulin standard (Bio-Rad Laboratories). SDS-PAGE analysis of all BER proteins is shown in Figure S1.

2.6 Global assessment of BER activity

The substrate was 25 nM duplex or NCP (0.5 pmol in a final volume of 20 μL). To assess UDG activity, the substrate was incubated for 1 h at 37 °C with 500 nM UDG in reaction buffer (20 nM Tris [pH 7.6], 50 mM NaCl, 150 mM KCl, 1 mM DTT, 5 mM $MgCl_2$, and 200 μg/mL BSA). To assess UDG and APE1 activity, the substrate was incubated for 1 h at 37 °C with 500 nM UDG and 500 nM APE1 in reaction buffer. To assess UDG, APE1, and Pol β activity, the substrate was incubated for 2 h at 37 °C with 500 nM UDG, 500 nM APE1, and 250 nM Pol β in reaction buffer supplemented with 100 μM dCTP (ThermoFisher Scientific). To assess UDG, APE1, Pol β, and LigIIIα/XRCC1 activity, the substrate was incubated for 2 h at 37 °C with 500 nM UDG, 500 nM APE1, 250 nM Pol β, and 250 nM LigIIIα/XRCC1 in reaction buffer supplemented with 100 μM dCTP and 1 mM ATP. A negative control (E) did not contain any added BER enzymes and reveals any pre-existing damage or damage caused by work up. All samples were quenched with equal volume of 1 M NaOH/50 mM EDTA also containing the 5'-^{32}P-radiolabeled internal standards. Samples incubated with only UDG were incubated at 90˚C for 5 min to cleave at any abasic sites. All samples were extracted with PCI and twice precipitated using precipitate solution and cold 200 proof ethanol. Pelleted samples were resuspended in 1:1 formamide:deionized water and split in half. Half of the sample was loaded onto a 10% denaturing PAGE gel to resolve nucleobases -131 to -82 while the other half was loaded onto an 8% denaturing PAGE gel to resolve nucleobases -75 to -12. Gels were imaged by phosphorimagery and quantified by SAFA.

The 27mer and 118mer internal standards were used as loading controls to normalize band intensities in each lane (27mer for positions -75 to -12; 118mer for positions -131 to -82). Background at each base position, as determined using the appropriate negative control (E), was then subtracted from the BER enzyme treated samples. At each location the ratio of corrected band intensity in NCP relative to free duplex DNA (FD) was calculated to obtain the ratio of product yield (P_{NCP}/P_{FD}) with n = 3-5 for each ratio. Activity level is defined as NCP/FD values of greater than or equal to 0.7, 0.7 < x < 0.2, or less than or equal to 0.2 as HIGH, MID, and LOW, respectively.

For Pol β, the ratio of product yield was determined by first finding the NCP fraction product:

$$F_{P(dCTP)} = \frac{\delta_I}{\delta_I + \delta_{U+A}}$$

where δ_I and δ_{U+A} represent the densities of the product and substrate bands, respectively, at each U location. The ratio of product yield for Pol β was determined as:

$$\frac{NCP}{FD} = \frac{F_{P(dCTP)} * Band\ Intensity\ APE1_{NCP}}{Band\ Intensity\ APE1_{duplex}}$$

For LigIIIα/XRCC1, the ratio of product yield was determined by first finding the NCP fraction product:

$$F_{P(Ligase)} = 1 - \frac{\delta_{Ligase}}{\delta_{Pol\beta}}$$

where δ_{Ligase} and $\delta_{Pol\beta}$ represent the densities of the product and substrate bands, respectively. The ratio of product yield was determined as:

$$\frac{NCP}{FD} = \frac{Band\ Intensity\ Pol\beta_{NCP} * F_{P(Ligase)}}{Band\ Intensity\ APE1_{duplex}}$$

Band intensity for the APE1 duplex control was used as the denominator instead of band intensity for Pol β duplex control because incorporation of multiple nucleotides by Pol β was observed at some sites in the duplex control which meant that the band intensity at each site could not be readily determined. The standard error (SE) of P_{NCP}/P_{FD} was calculated by $SE = \sigma/\sqrt{n}$ where σ is the standard deviation and n is sample size. A two-tailed Welch's t test ($\alpha = 0.05$) was performed to obtain p at each position. We considered $p < 0.05$ to be significant. All statistical analysis was performed using R.

2.7 Single-turnover kinetics experiments for Pol β and LigIIIα/XRCC1

For quantitative kinetic analysis of Pol β, 25 nM NCP was mixed with 500 nM UDG and 500 nM APE1 in 20 μL reaction buffer (20 nM Tris [pH 7.6], 50 mM NaCl, 150 mM KCl, 1 mM DTT, 5 mM $MgCl_2$, 100 μM dCTP, 200 μg/mL BSA) and incubated at 37 °C for 3 h. 250 nM Pol β was then added, incubated at 37 °C, and quenched after varying amount of time (1, 5, 15, 30, 60, or 120 min) by the addition of NaOH and EDTA (final concentrations of 500 and 25 mM, respectively) containing the 5'-^{32}P-radiolabeled internal standards. DNA fragments were extracted with PCI and twice precipitated using precipitate solution and cold 200 proof ethanol. Precipitated samples were resuspended in 1:1 formamide:deionized water and split in half. Half of the sample was loaded onto a 10% denaturing PAGE gel to resolve nucleobases -131 to -82 while the other half was loaded onto an 8% denaturing PAGE gel to resolve nucleobases -75 to -12. Gels were imaged by phosphorimagery and quantified by SAFA.

Using band intensities that had been corrected for background damage using (E), the fraction product for Pol β was determined for each time point, $F_P(t)$, using the following formula:

$$F_P(t) = \frac{\delta_P(t)}{\delta_P(t) + \delta_S(t)}$$

Where $\delta_P(t)$ and $\delta_S(t)$ represents the densities of the product and substrate bands at time (t). The mean product fraction was determined based on three replicates at each time point. Based on the averaged data, the time course of product fraction was fit to a single- or double- exponential model using the following formulas:

$$y(t) = y_{max}(1-e^{-k^{obs}t})$$

or

$$y(t) = y_{1max}(1-e^{-k^{obs}t}) + y_{2max}(1-e^{-k^{obs}t})$$

where y_{max} is the amplitude of the fit, k_{obs} is the observed rate constant, and t is time. The standard error (SE) was calculated by $SE = \sigma/\sqrt{n}$ where σ is the standard deviation and n is 3.

For quantitative kinetic analysis of LigIIIα/XRCC1, 25 nM NCP was mixed with 500 nM UDG, 500 nM APE1, and 375 nM Pol β in reaction buffer (same as above but supplemented with 1 mM ATP) and incubated at 37 °C for 3 h. 250 nM LigIIIα/XRCC1 was then added, incubated at 37 °C, and quenched after varying amount of time (1, 5, 15, 30, 60, or 120 min). Reaction quenching and sample work up was as described above for Pol β.

To determine the fraction product for LigIIIα/XRCC1 time courses, the fraction product at each timepoint, F_P, was determined using the following formula after background subtraction:

$$F_p = 1 - \frac{Band\ Intensity\ Unligated\ Product_{NCP}}{Band\ Intensity\ Pol\beta_{NCP}}$$

The standard error (SE) was calculated by $SE = \sigma/\sqrt{n}$ where σ is the standard deviation and n is 8.

3. Results and Discussion

3.1 Reconstitution of NCPs with global U substitution

To understand how BER enzymes initiate and complete repair on packaged DNA in chromatin, we prepared NCPs using the Widom 601 DNA sequence [30]. This DNA sequence binds to the histone octamer core in a single rotational and translational position, producing a homogenous population of positioned NCPs [31, 32]. U was used as a representative lesion that is repaired by the BER pathway and was incorporated into the "J strand" of the Widom 601 DNA (as defined in the crystal structure of Widom 601 NCPs) [31]. U was globally incorporated using chemical synthesis techniques to create 145 bp duplexes containing U:G bp, which mimics the deamination of a C:G bp. This global incorporation of U was accomplished using a mixture of C/U during chemical synthesis, as we reported previously [24]. The molar ratio of C/U was determined by a Poisson distribution to ensure that 95% of the DNA contains at most one U. The global incorporation of U allows us to probe BER at 27 unique rotational and translational positions in the NCPs to provide a broad view of repair in packaged DNA.

The DNA products generated by each of the BER enzymes have distinct migrations via denaturing PAGE. This migration pattern was leveraged to monitor the activity of each enzyme. Nevertheless, because the global population of U-containing NCPs is analyzed collectively, it would be challenging to differentiate enzymatic activity in regions of sequential bases (e.g., 5'-CC-3', 5'-CCC-3', etc. where any of the C could be replaced by U). Therefore, five cytosines in the Widom 601 J strand were replaced with other nucleobases (Scheme S1). This modified J strand is used in the work presented here and will be subsequently referred to as the J strand. Nucleobases

of the J strand are numbered from -1 to -145 from the 3'- to 5'-end. This numbering scheme was chosen to facilitate comparison to previously published repair fingerprinting data for DNA glycosylases acting on the I strand of 601 NCPs [24, 33-37]. We note that the -1 position of the J strand is base paired to position 1 of the I strand. The incorporation of U at the expected locations in the J strand was confirmed by cleavage of the global DNA by UDG (Figure S2).

NCPs were assembled following the salt-dialysis method using global U-containing DNA duplex and histone octamers [25]. The formation of NCPs was confirmed using native PAGE, where single-stranded and duplex DNA controls migrate faster than NCPs (Figure S3).

3.2 Determining rotational position of DNA using hydroxyl radical and DNase footprinting

To determine the rotational position of nucleobases in the NCPs, we used two complementary footprinting techniques: hydroxyl radical footprinting (HRF) [26, 38] and DNase footprinting [39]. For HRF, regions of the sugar-phosphate backbone that face outward toward solution (OUT) are highly susceptible to cleavage by hydroxyl radicals. In contrast, regions of the sugar-phosphate backbone that face in towards the histone core (IN) are physically sequestered and protected from cleavage. Nucleobases with rotational positioning between OUT and IN have intermediate reactivity towards hydroxyl radicals (MID). The resulting oscillating pattern created by this HRF determines the rotational positioning of each nucleobase (Figure S4, Table S1). Notably, the rotational positioning for the modified 601 DNA in an NCP is consistent with both HRF and crystal structures of NCPs containing the unmodified 601 DNA sequence [24, 31].

DNase footprinting uses an enzyme which is significantly larger than the hydroxyl radical (30,000 Da vs 17 Da) as a footprinting agent. This complementary technique contributes to our understanding of how BER enzymes access lesions throughout the NCP. The bands in a DNase footprinting gel represent cleavage at nucleobases that are accessible to DNase. For the NCPs used

in this work, cleavage is observed approximately every ten bp (these are regions identified as OUT by HRF), although with differing intensity reflecting the varying ability of DNase to access regions of DNA in the NCP (Figure S5).

3.3 Excision of U by the glycosylase UDG is correlated with rotational position

Having established the rotational position of each U in the NCPs, we next investigated the initiation of BER by the glycosylase UDG. Duplex DNA was used as a positive control and excision at every U site was observed by denaturing PAGE (Figure 2; FD, U lanes; Figure S6). Excision of U from NCPs is shown in Figure 2 (NCP, U lanes). Activity of UDG was then plotted as a ratio of product yield in NCPs relative to free duplex (NCP/FD) (Figure 3, blue bars; Table S2). A ratio of 1 would indicate that UDG excises U as efficiently from NCPs as from unpackaged DNA duplex.

Consistent with earlier reports, UDG excision activity is largely dependent on the rotational positioning of the lesion [24, 36, 40-47]. Most OUT sites exhibit high UDG activity and have NCP/FD ratios of at least 0.7 (sites -72, -82, -93, -113). High U excision is also observed at some MID sites (-18, -39, -84, -125). Significant inhibition of U excision is observed at other MID sites and all IN sites. Notably, site -62 is an OUT site that experiences low excision by UDG. Site -62 is in a region of the NCP that is known to experience severe kinking [32]. This kinking associated with a single-base pair register shift could impact UDG activity. Notably, DNase also does not have cleavage activity in this region (Figure S5).

Sites -12 to -24 and -121 to -131 are in the entry/exit region of the NCP. In this region, transient and spontaneous unwrapping of DNA from the histones may allow enzymes to access lesions that would otherwise be sterically occluded [19, 47-49]. However, except for sites -18, -

21, -125, and -127, NCP/FD values are less than 0.36. These data are consistent with rotational positioning being a major factor defining activity of UDG in these NCPs.

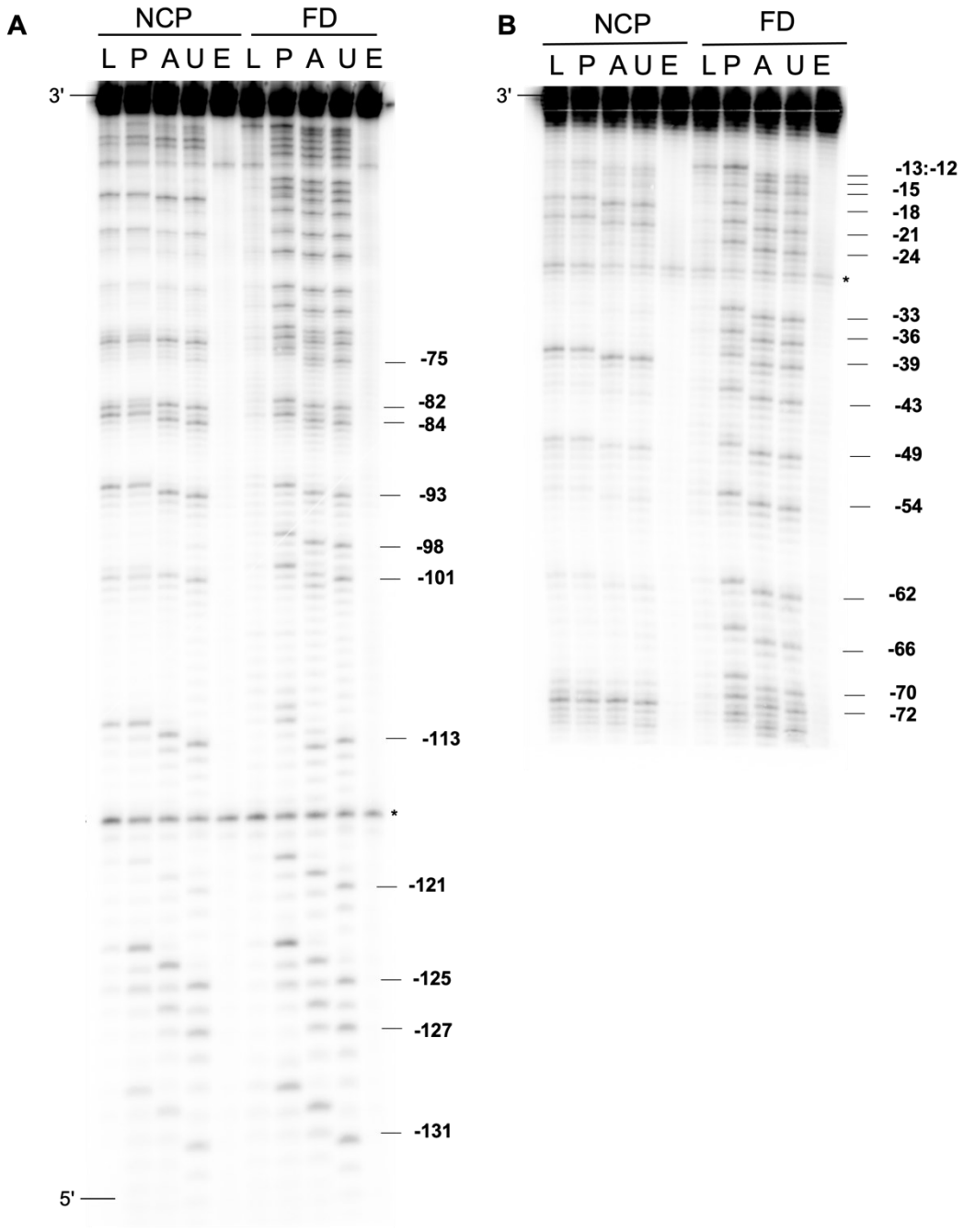

Figure 2. BER activity of UDG, APE1, Pol β, and LigIIIα/XRCC1 on Widom 601 duplex DNA and NCPs containing global C to U substitution. (A) Representative 10% denaturing PAGE following incubation of duplex DNA (FD) or NCPs with UDG (U lanes), UDG and APE1 (A lanes), UDG, APE1, and Pol β (P lanes), or UDG, APE1, Pol β and LigIIIα/XRCC1 (L lanes) (see Materials and Methods for experimental conditions). E lanes are samples that have undergone the same workup, but no BER enzymes are added. Internal standards are indicated with an asterisk. Bands

from site -131 to -75 were quantified by SAFA. (B) Same as panel A except 8% denaturing PAGE and bands from site -72 to -12 were quantified by SAFA.

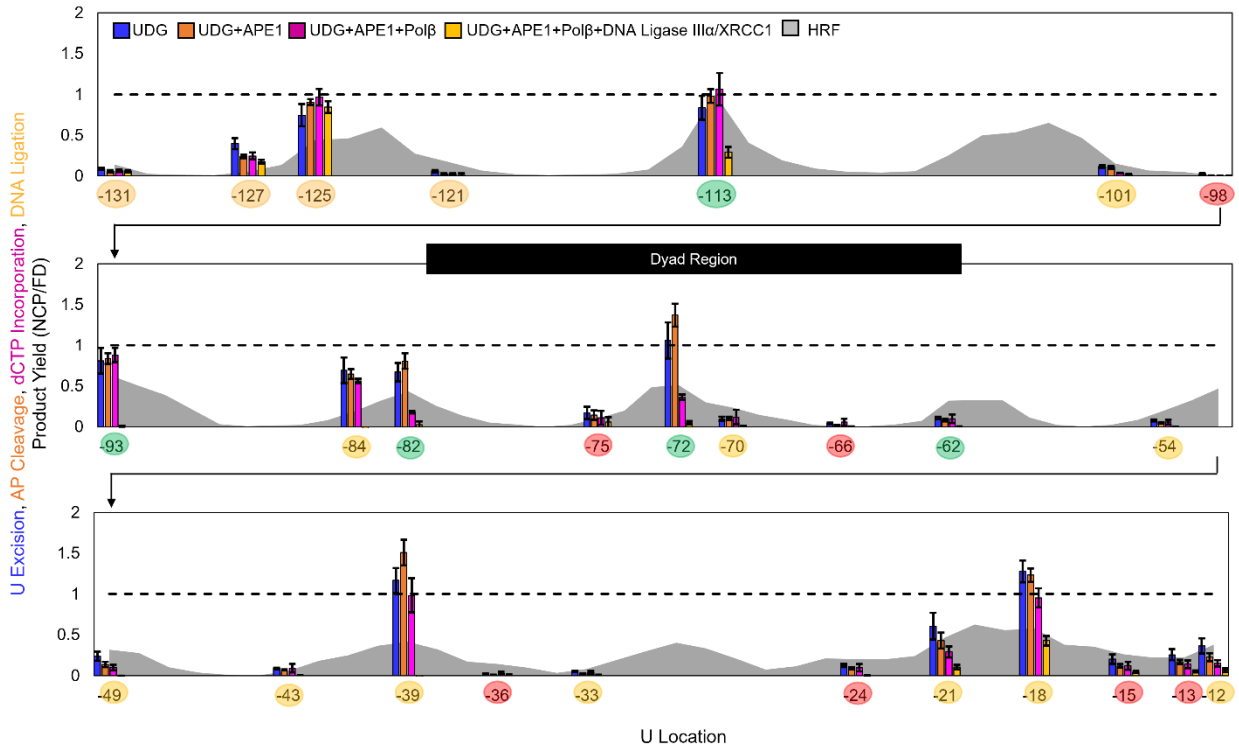

Figure 3. Relative activity of BER enzymes on NCPs containing global C to U substitution. At each U location, the ratio of product yield in NCPs to duplex DNA (FD) is plotted for UDG (blue), UDG and APE1 (orange), UDG, APE1, and dCTP incorporation by Pol β (pink), and UDG, APE1, Pol β, and LigIIIα/XRCC1 (yellow). A ratio of 1 is indicated as a dashed line and represents an instance in which activity on NCPs is as efficient as activity on duplex DNA. Error bars represent standard error (n = 3-5). Rotational position of each nucleobase is determined by HRF (gray area). Numbers indicate the U locations (labeled -1 to -145 from the 3'- to 5'-end) and are colored green (OUT), yellow (MID), or red (IN) to reflect the rotational positioning as determined from HRF. Dyad region is indicated.

3.4 APE1 effectively incises abasic sites generated by UDG

In the BER pathway, APE1 follows UDG and is responsible for incising the sugar-phosphate backbone adjacent to the abasic site. In Figure 2, the difference in migration between the product generated by UDG alone (U lanes) and both UDG and APE1 (A lanes) is visible for both free duplex controls (FD) and NCPs. The amount of APE1 activity was plotted as a ratio of product yield in NCPs relative to free duplex (Figure 3, orange bars; Table S2). There is no

statistical difference between UDG activity (blue bars) and APE1 activity (orange bars). This result indicates that APE1 works efficiently on NCPs and, in fact, the initial steps of the BER pathway are not limited by APE1 but rather is controlled by the ability of UDG to initiate the repair event by excising U.

This concept of a DNA glycosylase being a limiting step of BER is supported by previous research. Using free duplex DNA substrates and nuclear extracts as the source of BER enzymes, the rate of repairing U was reported to be limited by the initiating DNA glycosylase [50]. Also consistent with the results presented here, using purified BER enzymes and an oligonucleosome array of 12 NCPs, UDG and APE1 were found to digest U:G bp to completion [51]. In other work using a 12 NCP oligonucleosome array, both UDG and APE1 exhibited activity, although slower than in a mono-NCP substrate [52].

The mechanism by which APE1 accesses abasic sites in an NCP was revealed in recent cryo-electron microscopy structures [53]. Using Widom 601 NCPs, APE1 was found to use a sculpting mechanism to bend nucleosomal DNA and move the DNA away from the histones. APE1 being able to process completely the products generated by a DNA glycosylase would prevent the accumulation of abasic sites, which are deleterious intermediates in the repair pathway. Abasic sites are also known to crosslink with proteins[54] and the crosslinking is enhanced in NCPs because of the lysine-rich N-terminal tails of histones [55, 56]. In the experiments conducted in the current work, no significant level of radioactivity in the organic phase of PCI extractions was detected. This observation suggests that stable DNA-histone crosslinks are not forming under the experimental conditions and may reflect effective substrate-product channeling between the BER enzymes.

3.5 DNA Pol β nucleotide incorporation activity is correlated with translational position

We next investigated the ability of Pol β to incorporate dCTP into the single nucleotide gaps generated by the combined activity of UDG and APE1. Nucleotide incorporation is plotted as a ratio of product yield in NCPs relative to free duplex (Figure 3, pink bars). High nucleotide incorporation activity, with NCP/FD of at least 0.7, is observed at -125, -113, -93, -39, -18 (Table S3). When the nucleotide incorporation activity of Pol β is compared to that of UDG and APE1 (Figure 3, pink versus orange bars), a strong dependence on the translational position of the gap is observed. At sites -131 to -93 and -12 to -36, which comprise the ~40-50 bp at each end of the nucleosomal DNA, Pol β activity is comparable to the combined activity of UDG and APE1. However, activity of Pol β is diminished or inhibited in the central ~45 bp of nucleosomal DNA (sites -84 to -43). These results suggest that in the absence of additional cellular factors, BER in positioned NCPs may stall at the gap-filling step in the central region of DNA. Notably, native PAGE analysis reveals that the NCPs retain their integrity following incubation with the BER proteins (Figure S7).

In previous work, an influence of translational position of the gap on Pol β incorporation activity was observed when a few gaps sites were compared. Using NCPs assembled from 146 bp of the *L. variegatus* 5S rRNA gene, more nucleotide incorporation was observed at a gap 22 bp from the end of the DNA compared to 51 bp from the end [46]. Notably, this 5S DNA sequence is less constrained on the histone surface than Widom 601 DNA and has multiple translational positions. It was also shown that preincubation of NCPs with the chromatin architectural factor HMGB1 modestly stimulates the nucleotide incorporation by Pol β [57]. Using NCPs assembled using DNA containing a glucocorticoid receptor element bracketed by multiple, positioned TG-motifs, no Pol β incorporation activity was observed at a gap in the central region near the dyad axis [43]. In Widom 601 NCPs, Pol β exhibited increased incorporation activity at a gap near the

end of the DNA compared to gaps near the dyad axis [45]. The results presented in the current work provide a more comprehensive description of the gap-filling step and demonstrate the influence of translational position when comparing nucleotide incorporation at 27 sites in Widom 601 NCPs.

Interestingly, others have shown that lesions in NCPs are preferentially repaired by Pol β over other DNA polymerases [58]. Furthermore, in Widom 601 NCPs the short-patch BER pathway was used by Pol β and incorporation was limited to one deoxynucleotide [58]. This previous research also guided our decision to focus on short-patch BER in this work. Consistent with this previously published work [58], at site -113 we observe the incorporation of two deoxynucleotides by Pol β in the duplex controls but only one in the NCP substrates. Lastly, whereas Pol β was found to have a search footprint of ~24 bp in free DNA, studies using Widom 601 NCPs demonstrated that Pol β is not processive and this lack of productive processive searching is due to inhibition of nucleotide incorporation activity [59].

X-ray crystallography has demonstrated that significant structural rearrangements of the DNA occur when Pol β binds gap-containing oligonucleotides [60]. The templating strand is bent 90°. Such a structural rearrangement in an NCP, if achievable, would orient OUT facing gaps towards the histone core and this rearrangement has previously been hypothesized to reduce Pol β nucleotide incorporation near the dyad region [45]. Additionally, it may be difficult to achieve this structural rearrangement with histone-bound DNA. Indeed, using formaldehyde crosslinking of Widom 601 NCPs, it was demonstrated that transient and spontaneous unwrapping of the DNA from histones is important for Pol β nucleotide incorporation in the entry/exit regions [45].

Another factor when considering enzymatic activity on an NCP is that each histone protein contains an unstructured N-terminal tail. The tail of H3 has been shown to interact with DNA near

the dyad region [61] and one might consider that the presence of this tail could influence Pol β activity in this region. However, the removal of histone tails has been shown to have little or no influence on the activity of UDG, APE1, or Pol β [43]. This result suggests that the H3 tail is not the cause of decreased Pol β activity in the central region of DNA in NCPs but rather the diminished nucleotide incorporation is derived from the need for contacts to DNA and/or structural rearrangements that cannot occur in histone-bound DNA.

It is notable that while the nucleotide incorporation activity of Pol β is suppressed or inhibited the in the central region of NCPs, it has been shown that the 5'-dRP lyase activity of the enzyme in this region is robust [62]. Notably, the dRP lyase and nucleotide incorporation activities of Pol β are catalyzed by separate domains. Nucleotide incorporation requires more extensive interactions and distortions of the templating strand than lyase activity which may be the basis for the difference in activity for the two domains of Pol β on an NCP [62]. It was recently reported that the dRP lyase and nucleotide incorporation activities of Pol β are interlocked with nucleotide incorporation occurring in between the two steps required for dRP lyase activity [63]. While the experimental set up and conditions of the current work do not allow us to probe the order of events, it is interesting to consider if Pol β uses a similar mechanism on NCPs.

3.6 Quantitative characterization of position-dependent nucleotide incorporation activity of Pol β

Prior research has provided kinetic descriptions of glycosylase and APE1 activity on NCPs [16, 53]. However, less information is available about Pol β. To quantitatively characterize the activity of Pol β catalyzing nucleotide incorporation on NCPs, single-turnover (STO) kinetics experiments were conducted. Nucleotide gaps were generated by incubating the global U-containing NCPs with UDG and APE1. Pol β was then added and nucleotide incorporation was

monitored as a function of time (Figure 4, S8). In STO experiments, Pol β is present in excess over the NCP substrate and the data can be fit to obtain k_{obs}. Because the amount of Pol β is not limiting, the results are reflective of nucleotide incorporation rather than substrate binding. We note that the results in Figure 4A are for NCP substrates and are presented as fraction product as a function time. Rather than reflecting activity relative to the duplex control, as in Figure 3, these data reflect dCTP incorporation at gap sites in the NCP.

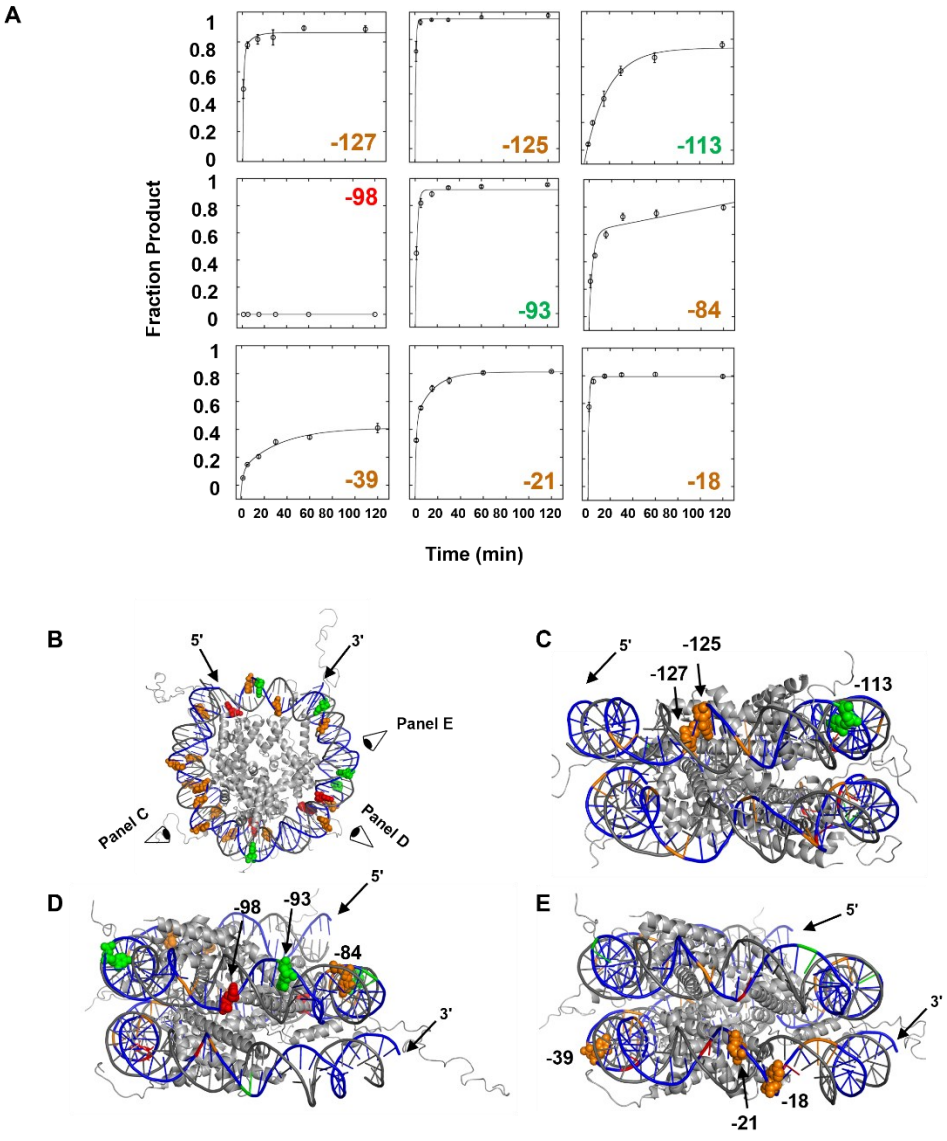

Figure 4. (A) Single-turnover kinetics time courses of Pol β nucleotide incorporation at a variety of sites in NCPs. Site and rotational position in the NCP are indicated by the numbers in green (OUT), orange (MID), and red (IN). Lines are the best fit to either mono- or biexponential growth models. Error bars represent the standard error (n = 3). (B) Representation of an NCP (as described in Figure 1B) with sites examined in panel A colored based on rotational positioning as OUT (green), MID (orange) and IN (red). (C, D, E) Views of the NCP from the perspectives indicated in panel B.

Pol β exhibits monophasic kinetics for nucleotide incorporation at some gaps (sites -125, -113, -93, -39 and -18) and biphasic kinetics at others (sites -127, -84, and -21) (Table S4). Monophasic kinetics indicates a single species while biphasic kinetics indicates two species with distinct incorporation rates. Multiphasic kinetics in NCPs have been observed previously for some DNA glycosylases[24, 40, 41, 47, 64] and APE1 [53]. Observing both monophasic and biphasic kinetics highlights how the unique microenvironments of the NCP impact Pol β incorporation activity.

The k_{obs} vary from 0.05 to 1.4 min^{-1} (comparing the rate for the major population for sites with biphasic kinetics). Previous reports of k_{obs} ranged from 0.12 min^{-1} to 10.8 min^{-1} for Pol β nucleotide incorporation under STO conditions at a few locations in Widom 601 NCPs [62, 65]. Interestingly, acetylation of H3 at lysine 14 or 56 was previously found to decrease the rate of nucleotide incorporation by 2-5-fold at a gap near the dyad [65].

When considering substrate-product channeling between BER enzymes, it has previously been shown that APE1 does not influence the rate of product formation by Pol β in Widom 601 NCPs under conditions with up to 10-fold excess of APE1 relative to Pol β [45]. However, LigIIIα/XRCC1 was previously shown to enhance the incorporation activity of Pol β on duplex[9] and at an IN facing gap in a 5S NCP [66]. We therefore examined Pol β incorporation activity in the presence of an equimolar and excess concentration of LigIIIα/XRCC1 (Figure S9). No statistically significant change in Pol β incorporation activity was observed at any gaps under either

condition on these Widom 601 NCPs (Figure S10). Notably, in the previous work where Pol β activity was enhanced in NCPs, the enhancement was due to disruption of the 5S NCPs at the IN facing gap by LigIIIα/XRCC1. No such disruption was reported for Widom 601 NCPs [66], suggesting that the DNA sequence may modulate the ability of LigIIIα/XRCC1 to influence nucleotide incorporation by Pol β.

3.7 Nick sealing by DNA ligase IIIα/XRCC1 observed in entry/exit regions of nucleosomal DNA

We next investigated the ability of LigIIIα/XRCC1 to catalyze nick sealing to complete the DNA repair event. Notably, successful completion of the repair event restores the full-length DNA sequence. Therefore, when visualized by denaturing PAGE, ligation activity (Figure 2, L lanes; Figure S11) manifests as the disappearance of the UDG/APE1/Pol β product (Figure 2, P lanes) and restoration of the full-length 145 bp product. High yield of ligation (NCP/FD of greater than 0.7) is observed only at site -125 (Table S3). However, when the activity of LigIIIα/XRCC1 is compared to the combined activity of UDG, APE1, and Pol β (Figure 3, yellow versus pink bars) ligation is observed at both entry/exit regions of the nucleosomal DNA (in the regions that are up to 33 and 22 bp from the two ends). While the overall amount of ligated product is low at some locations in the entry/exit regions, we note that excision of U by UDG, rather than LigIIIα/XRCC1 activity, is the limiting step in the repair. Partial ligation is observed at sites -113 and -18. No ligation is observed at some sites where Pol β has robust incorporation activity (-93, -84, and -39). Experiments were also conducted with increased concentrations of LigIIIα/XRCC1 and no change in ligation yield was observed (Figure S9, S10). As observed for Pol β, these results reflect a significant dependence on translational positioning for nick sealing by LigIIIα/XRCC1.

We note that in these experiments, UDG, APE1, Pol β, and LigIIIα/XRCC1 are present. Any substrate-product channeling or coordination between the BER enzymes would be feasible. For example, it was previously demonstrated that a Pol β/XRCC1 complex increases the processivity of the BER pathway after the incorporation activity of Pol β and enhances channeling of the nicked DNA to LigIIIα [67]. Complexation with XRCC1 has also been shown to modulate localization of Pol β to chromatin [68]. We also note that LigIIIα/XRCC1 activity requires removal of the 5'-dRP by Pol β. As described earlier, the 5'-dRP lyase activity of Pol β has been shown to be robust even in the central region of nucleosomal DNA where nick ligation is not observed. Therefore, it is likely that it is lack of LigIIIα/XRCC1 activity that is responsible for the stalling of repair in this region of the NCP.

Unlike the other enzymes in the BER pathway, LigIII is known to encircle DNA [69]. A "jackknife" model for LigIII has been proposed by Ellenberger and co-workers in which the enzyme is in an extended conformation prior to binding a nick. Upon binding a nick, there is a conformational change to encircle the DNA [70, 71]. By observing nick sealing activity at 27 locations in an NCP the results obtained here are consistent with ligation occurring when nick sites are transiently exposed in the entry/exit regions by unwrapping from the histone proteins. Notably, no disruption of Widom 601 NCPs was observed previously [66] or in this work, consistent instead with transient unwrapping modulating ligation activity.

3.8 Quantitative characterization of nick sealing in an NCP

To quantitatively characterize nick sealing by LigIIIα/XRCC1 we performed STO experiments. Nick-containing NCPs were generated by the addition of UDG, APE1, and Pol β. LigIIIα/XRCC1 was then added, and product formation was monitored as a function of time to obtain k_{obs} (Figure 5, S12). We were able to determine k_{obs} at sites -127 and -125. LigIIIα/XRCC1

displays monophasic kinetics at both sites with k_{obs} of 0.13 and 0.11 min^{-1} for -127 and -125, respectively. While previous reports observed biphasic kinetics for LigIIIα/XRCC1 activity on 5S NCPs [72], we observed monophasic kinetics in Widom 601 NCPs indicating a single species facilitated by transient unwrapping of DNA in the entry/exit regions.

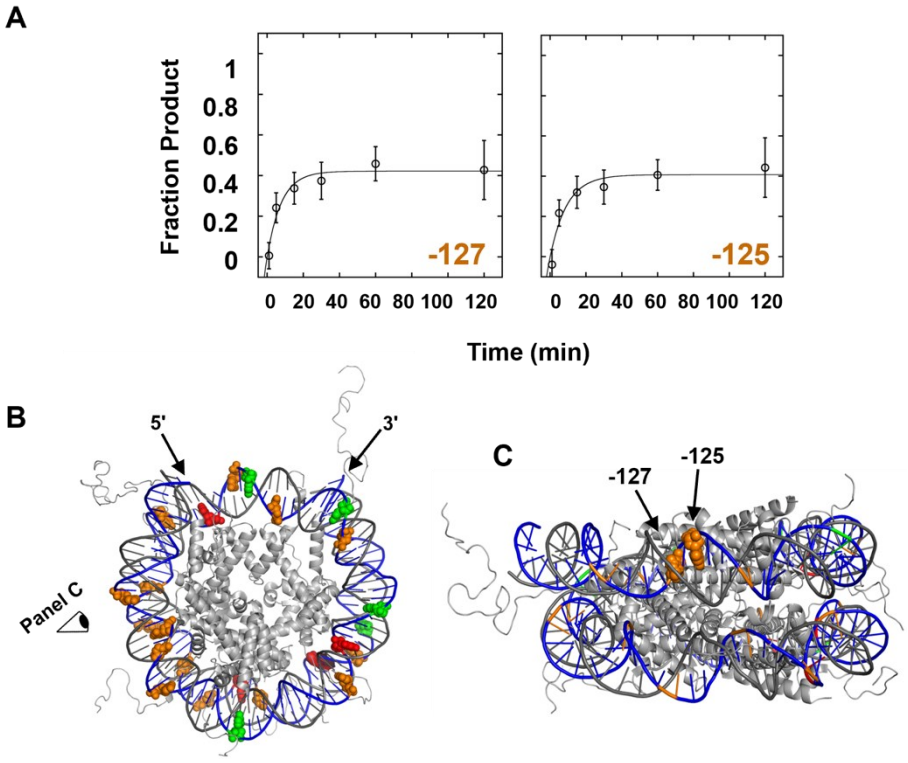

Figure 4. (A) Single-turnover kinetics time courses of LigIIIα/XRCC1 activity on NCPs. Site and rotational position in the NCP are indicated by the numbers in orange (MID). Lines are the best fit to a monoexponential growth model. Error bars represent the standard error (n=8). (B) Representation of an NCP (as described in Figure 1B) with sites examined in panel A colored based on rotational positioning. (C) View of the NCP from the perspective indicated in panel B.

4. Conclusions and Perspectives

In this work we investigated short-patch BER at 27 unique rotational and translational locations in a positioned NCP. This global analysis is summarized in Figure 6 and reveals that initiation of the DNA repair event, in this case by the glycosylase UDG, is dictated by the rotational

position of the lesion. APE1 can incise all the abasic sites generated by the DNA glycosylase but subsequent nucleotide incorporation by Pol β stalls in the central ~45 bp of the nucleosomal DNA. Lastly, nick ligation by LigIIIα/XRCC1 is achieved only in the entry/exit regions of nucleosomal DNA.

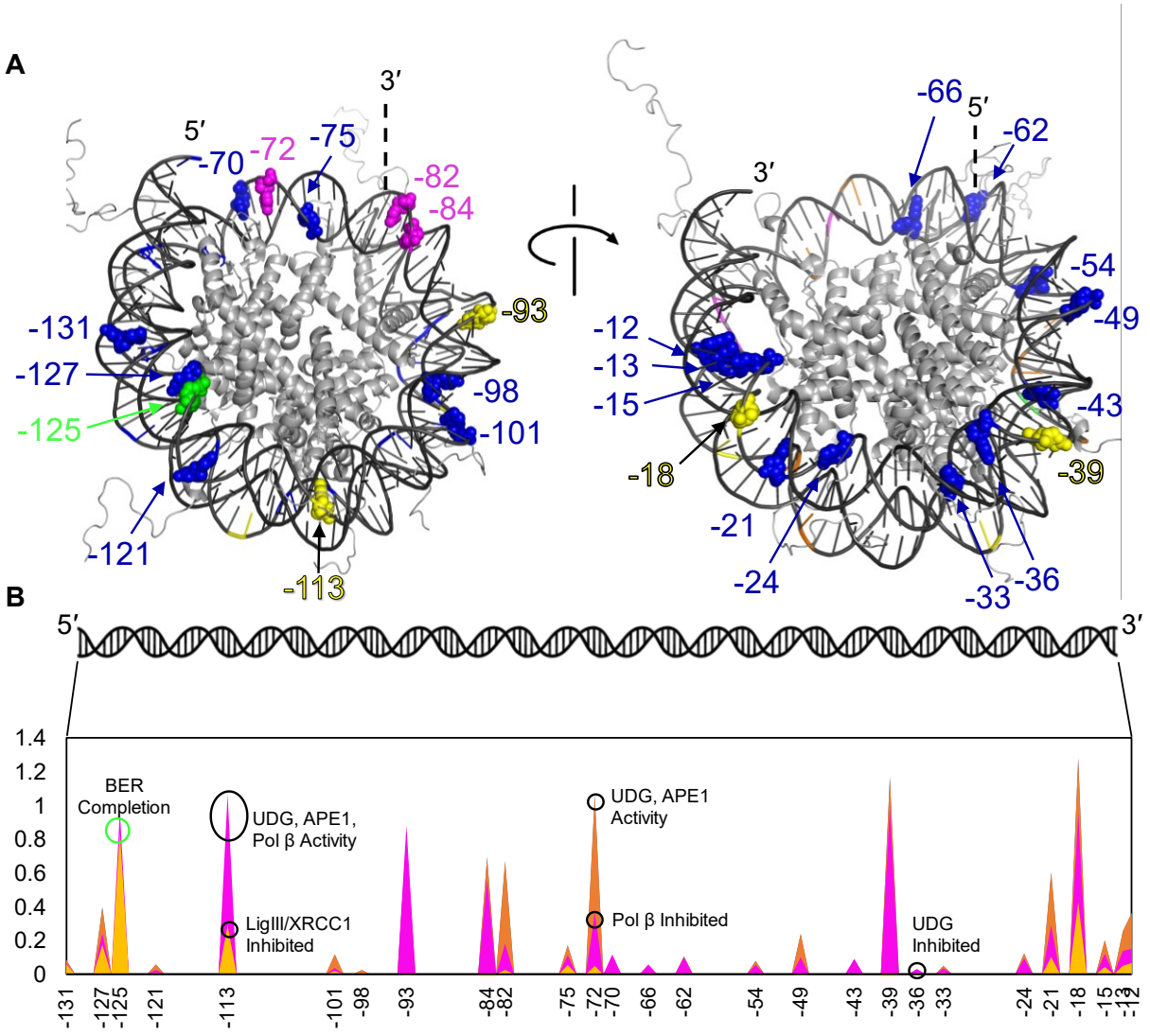

Figure 5. Summary of BER on a positioned NCP. (A) Mapping of U sites on the NCP. Color of U represents the first enzyme in the BER pathway that is inefficient and where BER stalls in the NCP (blue, UDG; pink, Pol β; yellow, LigIIIα/XRCC1). BER is successfully completed at -125 and this U is colored green. Left and right NCP are rotated by 180° along the axis indicated. (B) Extent of activity of each BER enzyme on the NCP. UDG activity (blue), APE1 (orange), Pol β nucleotide incorporation (pink), and LigIIIα/XRCC1 (yellow) are indicated. Overlapping colors indicate that the enzymes have similar activity. Black circles indicate one example each of a location where UDG, Pol β, and LigIIIα/XRCC1 are inhibited.

These results are consistent with genome-wide maps of DNA damage and mutations. Following exposure to a damaging agent known to create lesions repaired by BER, genome-wide maps reveal higher levels of lesions and increased mutation frequency in strongly-positioned nucleosomes compared to other regions of the genome [73]. Furthermore, both the translational and rotational position of lesions modulates their repair efficiency and mutation frequency, as observed in the current work. Notably, the highest levels of lesions and mutations were observed in the central region of nucleosomal DNA near the dyad axis which is also consistent with the results obtained here for global screening of BER in a positioned NCP.

Our biochemical analysis of BER in an NCP model system reveals the initiation and completion of repair in the absence of any external cellular factors. Notably, even in the absence of other cellular factors, robust BER is observed at site -125 of this positioned NCP. At other sites, the repair event is not initiated, due to lack of UDG activity, or is stalled mid-repair due to limited Pol β or LigIIIα/XRCC1 activity. There are many biological factors that may facilitate BER on chromatin *in vivo*. For instance, chromatin remodelers are a major mechanism for modulating the physical accessibility of DNA and can alter and disrupt DNA-histone contacts. These remodelers can drive NCPs to slide along DNA and can evict histones from the protein core and may provide BER enzymes access to DNA in chromatin. Indeed, the SWI/SNF chromatin remodeler was shown to stimulate excision of an 8-oxo-7,8-dihydroguanine lesion from Widom 601 NCPs [74]. Chromatin remodelers can also coordinate the exchange of canonical histones for histone variants, and we [24, 36] and others [74] have previously shown that several histone variants can facilitate excision of lesions by DNA glycosylases. It has also been reported that human cells contain a factor that can facilitate excision of a lesion by a DNA glycosylase and that this unknown factor(s) differs from most known chromatin remodelers [75]. A remarkable number of histone post-

translational modifications have also been identified. This highly dynamic histone code has drawn significant interest due to its correlation with chromatin states that can modulate the accessibility of DNA . There is also evidence that the poly(ADP-ribose) polymerase (PARP) family of enzymes can modulate the activity of BER enzymes [78-80]. The presence of PARP1 was shown to lead to decreased APE1, Pol β, and to a lesser extent LigIIIα/XRCC1 activity in an NCP. PARylation by PARP1 attenuated this effect. However, PARylation by PARP2 led to inhibition of Pol β and stimulation of LigIIIα/XRCC1 in an NAD^+-dependent manner [80]. The current research also relied on a DNA positioning sequence, which minimizes the heterogeneity of the NCPs to allow for interpretation of the results. While such positioning sequences are well documented *in vivo*, other regions of the genome are weakly positioned and is another factor that may influence their accessibility to BER enzymes.

The results described here begin to provide a chemically logical roadmap to understand how DNA damage relates to genomic instability and genetic change. Further research is needed to fully parse the factors that contribute to regulating BER in chromatin.

CRediT authorship contribution statement

Conceptualization, T.B.S., S.D.; Investigation, T.B.S.; Enzymatic assays, T.B.S.; Protein expression and purification, D.L.S., T.N.; Formal analysis, T.B.S., S.D.; Funding acquisition, J.B.S., A.E.T., S.D.; Resources; T.B.S., D.L.S., T.N.; Writing – Original Draft, T.B.S., S.D.; Review and Editing, T.B.S., D.L.S., T.N., J.B.S., A.E.T., S.D.; Supervision, J.B.S., A.E.T., S.D.

Acknowledgments

This work was supported by the National Science Foundation (MCB-2111680, S.D.) and by the National Institutes of Health (R01 CA281044-01A1, J.B.S.; R01 ES012512, A.E.T.; P01

CA92584, A.E.T PI Tainer). T.B.S. has been supported by training grants from the National Institute of General Medical Sciences (R25 GM083270) and National Institute of Environmental Health Sciences (T32 ES007272). D.L.S has been supported by the University of Arizona Integrative Cancer Scholar T32 (T32 CA009213) training grant from the National Cancer Institute. Any opinion, findings, and conclusions expressed in this work are those of the authors and do not necessarily reflect the views of the National Science Foundation or the National Institutes of Health.

Declaration of Competing Interest

The authors declare that they have no known competing financial interests or personal relationships that could have appeared to influence the work reported in this paper.

Appendix A. Supporting information

Supplementary data associated with this article can be found in the online version.

References

[1] S.S. David, V.L. O'Shea, S. Kundu, Base-excision repair of oxidative DNA damage, Nature, 447 (2007) 941-950.
[2] K.M. Schermerhorn, S. Delaney, A chemical and kinetic perspective on base excision repair of DNA, Acc. Chem. Res. , 47 (2014) 1238-1246.
[3] W.A. Beard, J.K. Horton, R. Prasad, S.H. Wilson, Eukaryotic base excision repair: new approaches shine light on mechanism, Annu. Rev. Biochem., 88 (2019) 137-162.
[4] W.A. Beard, R. Prasad, S.H. Wilson, Activities and mechanism of DNA polymerase β, Methods in Enzymology, 408 (2006) 91-107.
[5] S.H. Wilson, T.A. Kunkel, Passing the baton in base excision repair, Nature Structural Biology, 7 (2000) 176-178.
[6] M.S. Fairlamb, M. Spies, T.M. Washington, B.D. Freudenthal, Visualizing the coordination of apurinic/apyrimidinic endonuclease (APE1) and DNA Polymerase β during Base Excision Repair, J. Biol. Chem., 299 (2023) 104636.
[7] R. Prasad, D.D. Shock, W.A. Beard, S.H. Wilson, Substrate channeling in mammalian base excision repair pathways: passing the baton, J. Biol. Chem., 285 (2010) 40479-40488.

[8] A.E. Vidal, S. Boiteux, I.D. Hickson, J.P. Radicella, XRCC1 coordinates the initial and late stages of DNA abasic site repair through protein–protein interactions, The EMBO Journal, 20 (2001) 6530-6539.
[9] I.I. Dianova, K.M. Sleeth, S.L. Allinson, J.L. Parsons, C. Breslin, K.W. Caldecott, G.L. Dianov, XRCC1–DNA polymerase β interaction is required for efficient base excision repair, Nucleic Acids Research, 32 (2004) 2550-2555.
[10] M. Çağlayan, Interplay between DNA polymerases and DNA ligases: Influence on substrate channeling and the fidelity of DNA ligation, Journal of Molecular Biology, 431 (2019) 2068-2081.
[11] K.W. Caldecott, XRCC1 protein; Form and function, DNA Repair, 81 (2019) 102664.
[12] K. Luger, A.W. Mäder, R.K. Richmond, D.F. Sargent, T.J. Richmond, Crystal structure of the nucleosome core particle at 2.8 Å resolution, Nature, 389 (1997) 251.
[13] A. Valouev, S.M. Johnson, S.D. Boyd, C.L. Smith, A.Z. Fire, A. Sidow, Determinants of nucleosome organization in primary human cells, Nature, 474 (2011) 516-520.
[14] K. Brogaard, L. Xi, J.-P. Wang, J. Widom, A map of nucleosome positions in yeast at base-pair resolution, Nature, 486 (2012) 496-501.
[15] D.J. Gaffney, G. McVicker, A.A. Pai, Y.N. Fondufe-Mittendorf, N. Lewellen, K. Michelini, J. Widom, Y. Gilad, J.K. Pritchard, Controls of nucleosome positioning in the human genome, PLoS Genet, 8 (2012) e1003036.
[16] I.D. Odell, S.S. Wallace, D.S. Pederson, Rules of engagement for base excision repair in chromatin, Journal of Cellular Physiology, 228 (2013) 258-266.
[17] C. Li, S. Delaney, Challenges for base excision repair enzymes: Acquiring access to damaged DNA in chromatin, The Enzymes: DNA Repair, 45 (2019) 27-57.
[18] D.J. Biechele-Speziale, T.B. Sutton, S. Delaney, Obstacles and Opportunities for Base Excision Repair in Chromatin, DNA Repair, (2022) 103345.
[19] G. Li, J. Widom, Nucleosomes facilitate their own invasion, Nature Structural & Molecular Biology, 11 (2004) 763.
[20] T.T. Ngo, Q. Zhang, R. Zhou, J.G. Yodh, T. Ha, Asymmetric unwrapping of nucleosomes under tension directed by DNA local flexibility, Cell, 160 (2015) 1135-1144.
[21] A. Prasad, S.S. Wallace, D.S. Pederson, Initiation of base excision repair of oxidative lesions in nucleosomes by the human, bifunctional DNA glycosylase NTH1, Molecular and Cellular Biology, 27 (2007) 8442-8453.
[22] K. Bilotti, M.E. Tarantino, S. Delaney, Human oxoguanine glycosylase 1 removes solution accessible 8-oxo-7, 8-dihydroguanine lesions from globally substituted nucleosomes except in the dyad region, Biochemistry, 57 (2018) 1436-1439.
[23] B. Kavli, O. Sundheim, M. Akbari, M. Otterlei, H. Nilsen, F. Skorpen, P.A. Aas, L. Hagen, H.E. Krokan, G. Slupphaug, hUNG2 is the major repair enzyme for removal of uracil from U: A matches, U: G mismatches, and U in single-stranded DNA, with hSMUG1 as a broad specificity backup, J. Biol. Chem., 277 (2002) 39926-39936.
[24] C. Li, S. Delaney, Histone H2A variants enhance the initiation of base excision repair in nucleosomes, ACS Chem. Biol., 14 (2019) 1041-1050.
[25] K. Luger, T.J. Rechsteiner, T.J. Richmond, Expression and purification of recombinant histones and nucleosome reconstitution, in: Chromatin protocols, Springer, 1999, pp. 1-16.
[26] S.S. Jain, T.D. Tullius, Footprinting protein–DNA complexes using the hydroxyl radical, Nature Protocols, 3 (2008) 1092.

[27] R. Das, A. Laederach, S.M. Pearlman, D. Herschlag, R.B. Altman, SAFA: semi-automated footprinting analysis software for high-throughput quantification of nucleic acid footprinting experiments, RNA, 11 (2005) 344-354.
[28] B.E. Eckenroth, J.B. Towle-Weicksel, J.B. Sweasy, S. Doublié, The E295K cancer variant of human polymerase β favors the mismatch conformational pathway during nucleotide selection, J. Biol. Chem., 288 (2013) 34850-34860.
[29] I. Rashid, M.-S. Tsai, A. Sverzhinsky, A.S. Hlaing, B. Shih, A.C. Thwin, J.G. Lin, S.S. Maw, J.M. Pascal, A.E. Tomkinson, Purification and Characterization of Human DNA Ligase IIIα Complexes After Expression in Insect Cells, in: DNA Damage Responses: Methods and Protocols, Springer, 2022, pp. 243-269.
[30] P. Lowary, J. Widom, New DNA sequence rules for high affinity binding to histone octamer and sequence-directed nucleosome positioning, Journal of Molecular Biology, 276 (1998) 19-42.
[31] D. Vasudevan, E.Y. Chua, C.A. Davey, Crystal structures of nucleosome core particles containing the '601'strong positioning sequence, Journal of Molecular Biology, 403 (2010) 1-10.
[32] E.Y. Chua, D. Vasudevan, G.E. Davey, B. Wu, C.A. Davey, The mechanics behind DNA sequence-dependent properties of the nucleosome, Nucleic Acids Research, 40 (2012) 6338-6352.
[33] E.E. Kennedy, C. Li, S. Delaney, Global Repair Profile of Human Alkyladenine DNA Glycosylase on Nucleosomes Reveals DNA Packaging Effects, ACS Chem. Biol., 14 (2019) 1687-1692.
[34] P.J. Caffrey, R. Kher, K. Bian, D. Li, S. Delaney, Comparison of the Base Excision and Direct Reversal Repair Pathways for Correcting 1, N 6-Ethenoadenine in Strongly Positioned Nucleosome Core Particles, Chem. Res. Toxicol., 33 (2020).
[35] P.J. Caffrey, S. Delaney, Nucleosome Core Particles Lacking H2B or H3 Tails Are Altered Structurally and Have Differential Base Excision Repair Fingerprints, Biochemistry, 60 (2021) 210-218.
[36] C. Li, K.L. Rioux, S. Delaney, Histone Variants H3. 3 and H2A. Z/H3. 3 Facilitate Excision of Uracil from Nucleosome Core Particles, DNA Repair, 116 (2022) 103355.
[37] K.L. Rioux, S. Delaney, Ionic Strength Modulates Excision of Uracil by SMUG1 from Nucleosome Core Particles, DNA Repair, 125 (2023) 103482.
[38] B. Balasubramanian, W.K. Pogozelski, T.D. Tullius, DNA strand breaking by the hydroxyl radical is governed by the accessible surface areas of the hydrogen atoms of the DNA backbone, Proc. Natl. Acad. Sci. U. S. A., 95 (1998) 9738-9743.
[39] M. Brenowitz, D.F. Senear, M.A. Shea, G.K. Ackers, [9] Quantitative DNase footprint titration: A method for studying protein-DNA interactions, in: Methods in Enzymology, Elsevier, 1986, pp. 132-181.
[40] E.D. Olmon, S. Delaney, Differential ability of five DNA glycosylases to recognize and repair damage on nucleosomal DNA, ACS Chem. Biol., 12 (2017) 692-701.
[41] M.E. Tarantino, B.J. Dow, A.C. Drohat, S. Delaney, Nucleosomes and the three glycosylases: High, medium, and low levels of excision by the uracil DNA glycosylase superfamily, DNA Repair, 72 (2018) 56-63.
[42] H.A. Cole, J.M. Tabor-Godwin, J.J. Hayes, Uracil DNA glycosylase activity on nucleosomal DNA depends on rotational orientation of targets, J. Biol. Chem., 285 (2010) 2876-2885.
[43] B.C. Beard, S.H. Wilson, M.J. Smerdon, Suppressed catalytic activity of base excision repair enzymes on rotationally positioned uracil in nucleosomes, Proc. Natl. Acad. Sci. U. S. A., 100 (2003) 7465-7470.

[44] J.M. Hinz, Y. Rodriguez, M.J. Smerdon, Rotational dynamics of DNA on the nucleosome surface markedly impact accessibility to a DNA repair enzyme, Proc. Natl. Acad. Sci. U. S. A., 107 (2010) 4646-4651.
[45] Y. Rodriguez, M.J. Smerdon, The structural location of DNA lesions in nucleosome core particles determines accessibility by base excision repair enzymes, J. Biol. Chem., 288 (2013) 13863-13875.
[46] H. Nilsen, T. Lindahl, A. Verreault, DNA base excision repair of uracil residues in reconstituted nucleosome core particles, The EMBO Journal, 21 (2002) 5943-5952.
[47] Y. Ye, M.R. Stahley, J. Xu, J.I. Friedman, Y. Sun, J.N. McKnight, J.J. Gray, G.D. Bowman, J.T. Stivers, Enzymatic excision of uracil residues in nucleosomes depends on the local DNA structure and dynamics, Biochemistry, 51 (2012) 6028-6038.
[48] G. Li, M. Levitus, C. Bustamante, J. Widom, Rapid spontaneous accessibility of nucleosomal DNA, Nature Structural & Molecular Biology, 12 (2005) 46.
[49] R.L. Maher, A. Prasad, O. Rizvanova, S.S. Wallace, D.S. Pederson, Contribution of DNA unwrapping from histone octamers to the repair of oxidatively damaged DNA in nucleosomes, DNA Repair, 12 (2013) 964-971.
[50] T. Visnes, M. Akbari, L. Hagen, G. Slupphaug, H.E. Krokan, The rate of base excision repair of uracil is controlled by the initiating glycosylase, DNA Repair, 7 (2008) 1869-1881.
[51] S. Nakanishi, R. Prasad, S.H. Wilson, M. Smerdon, Different structural states in oligonucleosomes are required for early versus late steps of base excision repair, Nucleic Acids Research, 35 (2007) 4313-4321.
[52] D.R. Banerjee, C.E. Deckard III, M.B. Elinski, M.L. Buzbee, W.W. Wang, J.D. Batteas, J.T. Sczepanski, Plug-and-play approach for preparing chromatin containing site-specific DNA modifications: The influence of chromatin structure on base excision repair, J. Am. Chem. Soc., 140 (2018) 8260-8267.
[53] T.M. Weaver, N.M. Hoitsma, J.J. Spencer, L. Gakhar, N.J. Schnicker, B.D. Freudenthal, Structural basis for APE1 processing DNA damage in the nucleosome, Nature Communications, 13 (2022) 5390.
[54] P.S. Thompson, D. Cortez, New insights into abasic site repair and tolerance, DNA Repair, 90 (2020) 102866.
[55] J.T. Sczepanski, R.S. Wong, J.N. McKnight, G.D. Bowman, M.M. Greenberg, Rapid DNA–protein cross-linking and strand scission by an abasic site in a nucleosome core particle, Proc. Natl. Acad. Sci. U. S. A., 107 (2010) 22475-22480.
[56] R. Wang, K. Yang, S. Banerjee, M.M. Greenberg, Rotational effects within nucleosome core particles on abasic site reactivity, Biochemistry, 57 (2018) 3945-3952.
[57] A. Balliano, F. Hao, C. Njeri, L. Balakrishnan, J.J. Hayes, HMGB1 stimulates activity of polymerase β on nucleosome substrates, Biochemistry, 56 (2017) 647-656.
[58] R. Meas, M.J. Smerdon, Nucleosomes determine their own patch size in base excision repair, Scientific Reports, 6 (2016) 27122.
[59] M.J. Howard, Y. Rodriguez, S.H. Wilson, DNA polymerase β uses its lyase domain in a processive search for DNA damage, Nucleic Acids Research, 45 (2017) 3822-3832.
[60] W.A. Beard, S.H. Wilson, Structure and mechanism of DNA polymerase β, Biochemistry, 53 (2014) 2768-2780.
[61] E.A. Morrison, S. Bowerman, K.L. Sylvers, J. Wereszczynski, C.A. Musselman, The conformation of the histone H3 tail inhibits association of the BPTF PHD finger with the nucleosome, Elife, 7 (2018) e31481.

[62] Y. Rodriguez, M.J. Howard, M.J. Cuneo, R. Prasad, S.H. Wilson, Unencumbered Pol β lyase activity in nucleosome core particles, Nucleic Acids Research, 45 (2017) 8901-8915.
[63] A. Kumar, A.J. Reed, W.J. Zahurancik, S.M. Daskalova, S.M. Hecht, Z. Suo, Interlocking activities of DNA polymerase β in the base excision repair pathway, Proceedings of the National Academy of Sciences, 119 (2022) e2118940119.
[64] K. Bilotti, E.E. Kennedy, C. Li, S. Delaney, Human OGG1 activity in nucleosomes is facilitated by transient unwrapping of DNA and is influenced by the local histone environment, DNA Repair, 59 (2017) 1-8.
[65] Y. Rodriguez, J.M. Hinz, M.F. Laughery, J.J. Wyrick, M.J. Smerdon, Site-specific acetylation of histone H3 decreases polymerase β activity on nucleosome core particles in vitro, J. Biol. Chem., 291 (2016) 11434-11445.
[66] I.D. Odell, J.-E. Barbour, D.L. Murphy, J.A. Della-Maria, J.B. Sweasy, A.E. Tomkinson, S.S. Wallace, D.S. Pederson, Nucleosome disruption by DNA ligase III-XRCC1 promotes efficient base excision repair, Molecular and Cellular Biology, 31 (2011) 4623-4632.
[67] Q. Tang, M. Çağlayan, The scaffold protein XRCC1 stabilizes the formation of polβ/gap DNA and ligase IIIα/nick DNA complexes in base excision repair, J. Biol. Chem., 297 (2021).
[68] Q. Fang, J. Andrews, N. Sharma, A. Wilk, J. Clark, J. Slyskova, C.A. Koczor, H. Lans, A. Prakash, R.W. Sobol, Stability and sub-cellular localization of DNA polymerase β is regulated by interactions with NQO1 and XRCC1 in response to oxidative stress, Nucleic Acids Research, 47 (2019) 6269-6286.
[69] J.M. Pascal, P.J. O'brien, A.E. Tomkinson, T. Ellenberger, Human DNA ligase I completely encircles and partially unwinds nicked DNA, Nature, 432 (2004) 473.
[70] E. Cotner-Gohara, I.-K. Kim, A.E. Tomkinson, T. Ellenberger, Two DNA-binding and nick recognition modules in human DNA ligase III, J. Biol. Chem., 283 (2008) 10764-10772.
[71] E. Cotner-Gohara, I.-K. Kim, M. Hammel, J.A. Tainer, A.E. Tomkinson, T. Ellenberger, Human DNA ligase III recognizes DNA ends by dynamic switching between two DNA-bound states, Biochemistry, 49 (2010) 6165-6176.
[72] W.J. Cannan, I. Rashid, A.E. Tomkinson, S.S. Wallace, D.S. Pederson, The Human Ligase IIIα-XRCC1 Protein Complex Performs DNA Nick Repair after Transient Unwrapping of Nucleosomal DNA, J. Biol. Chem., 292 (2017) 5227-5238.
[73] P. Mao, A.J. Brown, E.P. Malc, P.A. Mieczkowski, M.J. Smerdon, S.A. Roberts, J.J. Wyrick, Genome-wide maps of alkylation damage, repair, and mutagenesis in yeast reveal mechanisms of mutational heterogeneity, Genome Research, 27 (2017) 1674-1684.
[74] H. Menoni, D. Gasparutto, A. Hamiche, J. Cadet, S. Dimitrov, P. Bouvet, D. Angelov, ATP-dependent chromatin remodeling is required for base excision repair in conventional but not in variant H2A. Bbd nucleosomes, Molecular and Cellular Biology, 27 (2007) 5949-5956.
[75] R. Maher, C. Marsden, A. Averill, S. Wallace, J. Sweasy, D. Pederson, Human cells contain a factor that facilitates the DNA glycosylase-mediated excision of oxidized bases from occluded sites in nucleosomes, DNA Repair, 57 (2017) 91-97.
[76] Y. Rodriguez, J.K. Horton, S.H. Wilson, Histone H3 lysine 56 acetylation enhances AP endonuclease 1-mediated repair of AP sites in nucleosome core particles, Biochemistry, 58 (2019) 3646-3655.
[77] D.R. Banerjee, C.E. Deckard, Y. Zeng, J.T. Sczepanski, Acetylation of the histone H3 tail domain regulates base excision repair on higher-order chromatin structures, Scientific Reports, 9 (2019) 1-11.

[78] K.W. Caldecott, Mammalian single-strand break repair: mechanisms and links with chromatin, DNA Repair, 6 (2007) 443-453.
[79] K.H. Almeida, R.W. Sobol, A unified view of base excision repair: lesion-dependent protein complexes regulated by post-translational modification, DNA Repair, 6 (2007) 695-711.
[80] M. Kutuzov, E. Belousova, T. Kurgina, A. Ukraintsev, I. Vasil'Eva, S. Khodyreva, O. Lavrik, The contribution of PARP1, PARP2 and poly (ADP-ribosyl) ation to base excision repair in the nucleosomal context, Scientific Reports, 11 (2021) 4849.